Electronic Supplementary Material (ESI) for Energy & Environmental Science.

Supporting Information for

Fully-Integrated Electrochemical System that Captures CO_2 from Flue Gas to Produce Value-Added Chemicals at Ambient Conditions

Aditya Prajapati[1], Rohan Sartape[1], Miguel T. Galante[2], Jiahan Xie[3], Samuel Leung[3], Ivan Bessa[2], Marcio H. S. Andrade[2], Robert T. Somich[3], Marcio V. Reboucas[2], Gus T. Hutras[3], Nathalia Diniz[2], Meenesh R. Singh[1*]

[1] Department of Chemical Engineering, University of Illinois at Chicago, 929 W. Taylor St., Chicago, Illinois, USA 60607
[2] Braskem America Inc., 550 Technology Drive, Pittsburgh, PA, 15219
[3] Braskem S.A, Rua Eteno S/N, Camaçari, Bahia, Brazil

Table of Contents

S1. Experimental methods

This section describes the details of materials and chemicals used in this work, 3D printing and fabrication of the electrochemical cells used for both CO_2 capture and reduction processes, and the GC and HPLC methods for quantifying the CO_2 reduction products.

S1.1 Materials

Table S 1 shows the list of all the consumable items, their purity, and the source used in the CO_2 capture and reduction experiments.

Table S 1: List of chemicals and materials used for the experiments conducted in this work

Materials	Source
3D printing clear resin (RS-F2-GPCL-04)	FormLabs
KCl (99.999%)	Sigma Aldrich
KOH (>85%)	Sigma Aldrich
$KHCO_3$ (99.99%)	Sigma Aldrich
DI water (HPLC Grade)	Sigma Aldrich
Choline Hydroxide (46 wt%)	Sigma Aldrich
Ethylene Glycol (99.9%)	Renowned Trading, LLC
Carbon paper (Toray 060)	Fuel Cell Store
Cu mesh	FindProLabs, Zhejiang
CO_2 (99.99%)	Praxair
N_2 (99.99%)	Praxair

S1.2 Fabrication of devices

The 3D models of the different parts of the MAMG CO_2 capture setup and CO2RR setup were designed in SolidWorks® (2018, Dassault Systems) and then 3D printed using a stereolithography (SLA) 3D printer (Form 2, Formlabs Inc., USA). A clear FLGPCL02 resin activated by a 405 nm laser was used to 3D print optically clear microfluidic devices with 150 µm of lateral and 25 µm of axial resolutions. The clear resin was chemically resistant to various solvents in a wide range of pH 0-14. The printed parts were washed with isopropyl alcohol (IPA) (90%, Sigma-Aldrich) bath for 20 mins in the Form Wash (Formlabs Inc., USA) to remove the residues of the resin from the external surface. The post-washed 3D printed device was finished by removing supports and curing for 20 minutes in the Form Cure. (Formlabs Inc., USA). The optical transparency of the 3D printed ED device was improved by wet sanding using 400 to 12000 grit pads, followed by spray painting of resin.

S1.3 Electrochemical CO2RR experiments

All the experiments were performed in this 3D-printed cell. The resin used is resistant to harsh chemical environments. All the experiments are performed at room temperature. The cell consists of working of volume 2 ml with a recirculating reservoir of volume 30 ml and a counter compartment of volume 6 ml separated by SnowPure Excellion I200 anion exchange membrane (AEM) of 0.33-0.35 mm dry membrane thickness. The AEM is a quaternary ammonium-based membrane and a polymeric backbone supplied in Cl^- form that is ideal for the electrolyte used in the CO2RR experiments in this work. A Pt strip was used as the counter electrode in the counter compartment. In the working compartment, an Ag/AgCl micro-reference electrode was inserted. The overall applied potential to the working electrode was determined by:

$$V_{actual} = V_{applied} + 0.205 + 0.059 \times pH \qquad (1)$$

Before initiating the electrochemical measurements, CO_2 was sparged into the electrolyte reservoir at 50 sccm for at least 45 mins to saturate the electrolyte with CO_2. The saturation was monitored by observing the change in the pH of the electrolyte using a Versa Star Pro pH probe. At saturation, the pH of the electrolyte was steady at 6.19. Once the steady pH was reached, the electrolyte was recirculated using chemically inert Viton tubing through a MasterFlex peristaltic pump at 20 ml/min. The CO_2 sparging in the electrolyte was maintained throughout the experiment to maintain a high concentration of CO_2 in the electrolyte.

S1.4 Product distribution analysis for CO2RR

The CO2RR products were quantified using chromatographic techniques. The gaseous products evolved from CO2RR such as H_2, CO, CH_4, and C_2H_4 are quantified using gas chromatography (GC). The liquid products such as HCOOH, C_2H_5OH, and C_3H_7OH were quantified using high-pressure liquid chromatography (HPLC).

_GC:_ Gaseous products were quantified using an SRI 8610C GC MG#5. At the interval of 15 minutes, the gaseous products evolved were detected by passing the outlet from the electrochemical cell to the GC with argon as the carrier gas, and the product detection was done through thermal conductivity detector (TCD) and flame ionization detector (FID). The product gases in the GC were passed through two size-exclusion columns, Mol-sieve 8A and HaySep D. HaySep D efficiently separates larger molecules like C_2H_4. Smaller molecules like H_2 (from HER), CO, and CH_4 were separated through Mol-sieve 8A. The hydrocarbons were detected using FID, and non-hydrocarbon products were detected using TCD.

HPLC: The quantification of liquid products of CO_2 reduction was performed using High-pressure liquid chromatography (HPLC) on Agilent Infinity 1260 II HPLC with a $300mm \times 7.5mm$ Agilent Hi-plex- H column and a refractive index detector (RID). An isocratic elution of 1mM H_2SO_4 mobile phase was established at 0.6 mL/min. The column temperature was set to 60 °C, and the RID temperature was set to 35 °C. For each sample analysis with a total run time of 30 mins, a 10 μL sample was injected into the system through an autosampler. This operating method was developed by observing the retention times of the electrolyte and the possible CO_2 reduction products: HCOOH, HCHO, CH_3OH, CH_3COCH_3, CH_3COOH, C_2H_5OH, and $C_2H_2O_4$ so that none of the peaks overlap with each other in the shortest run time.

S2. Working principle of the migration-assisted moisture-gradient CO_2 capture process

Figure S 1 shows a detailed schematic of the entire process. CO_2 is sparged into the organic side, where it is chemisorbed by the 1.2M KOH solution in CO2BOL to form HCO_3^-. An anion exchange membrane (AEM) separates the organic side from the aqueous, initially comprising 0.1M KOH. The separation of the organic and aqueous sides creates a moisture gradient across the AEM, which initially drives the HCO_3^- diffusion across the AEM.

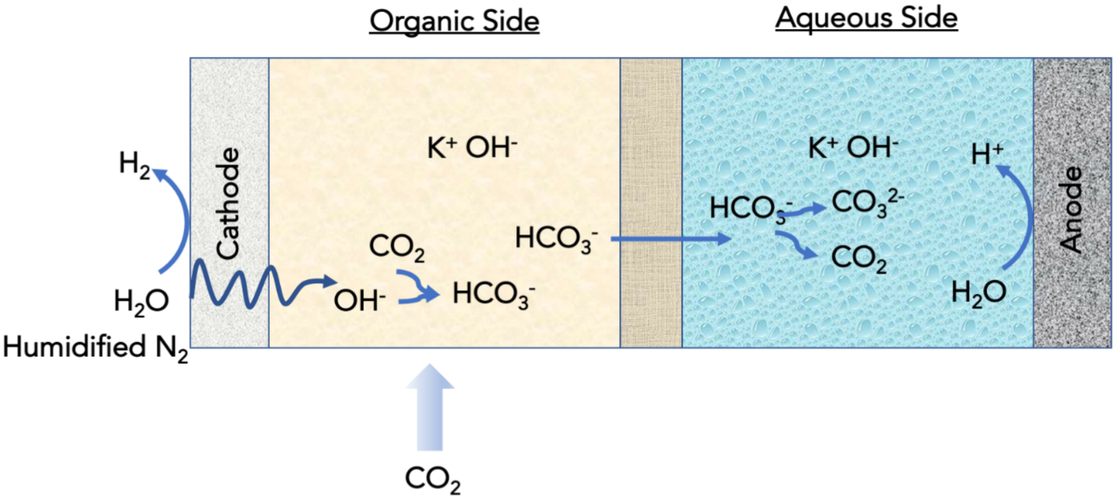

Figure S 1: A detailed schematic of MAMG process, where electrodialysis occurs across an anion exchange membrane (AEM)

On the aqueous side, the diffused HCO_3^- converts back to CO_2 and CO_3^{2-} thereby reducing the pH of the alkaline aqueous medium. This moisture-gradient facilitated transfer of HCO_3^- is accelerated by establishing an electric field across the device. The carbon paper cathode on the organic side is supplied with humidified N_2 and acts as a gas diffusion electrode to reduce water to H_2 and serves as a constant source to generate OH^- thereby increasing the CO_2 uptake. The aqueous side is anodic and attracts the HCO_3^- ions, further enhancing the rate of transfer of HCO_3^- and CO_2 release on the aqueous side.

The MAMG CO_2 capture can be implemented in a conventional electrodialysis stack as shown in Fig. S2. Here, an alternating pair of AEM and bipolar membrane (BPM) are implemented to transfer HCO_3^- from organic solution to aqueous solution selectively. There are several advantages of the electrodialysis stack as compared to the single membrane process shown in Fig. S1. For example, the O_2 from the anode and pure CO_2 in the aqueous solution is separated, and the cathodic reaction can be conducted separately without bringing the organic solution in contact with electrodes.

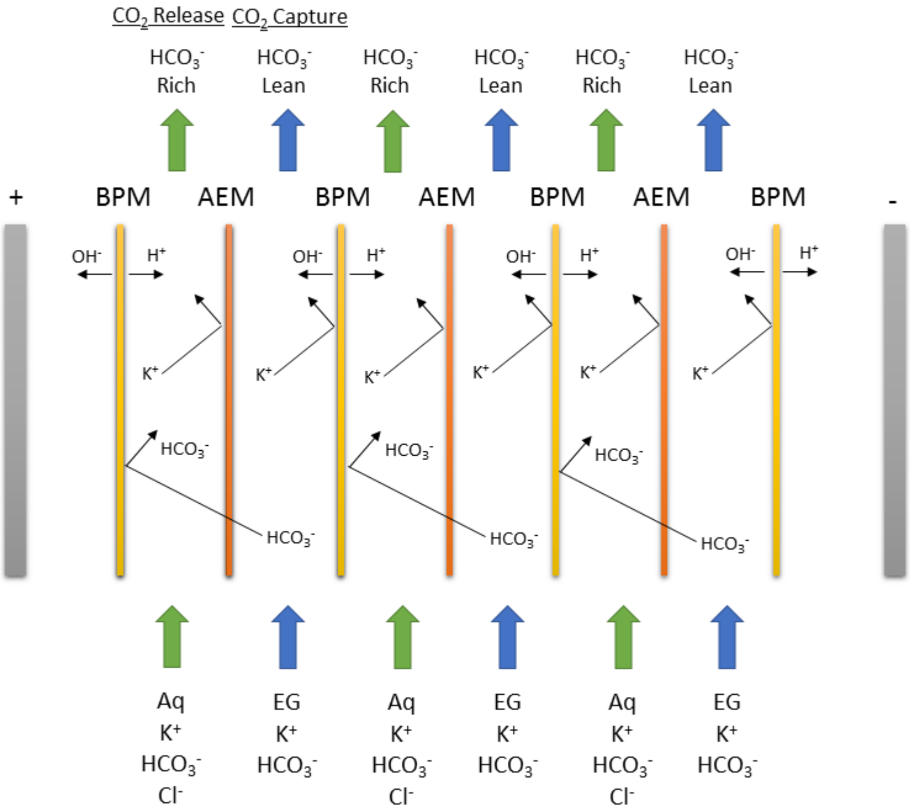

Figure S 2: Schematic of MAMG process implemented in an electrodialysis stack

Assessment of mass-transfer limitations in the MAMG CO_2 capture process: The MAMG process has four sequential processes – i) Absorption of CO_2: mass transfer of CO_2 from gas bubbles into the organic solution, ii) Formation of HCO_3^-:reaction of absorbed CO_2 with OH^- to produce HCO_3^-, and iii) Migration of HCO_3^-: migration of HCO_3^- from organic to the aqueous solution, and iv) Hydrolysis of HCO_3^- : reaction of HCO_3^- and H_2O to release CO_2. The acid-base reactions, such as the Formation and Hydrolysis of HCO_3^- (process ii and iv) are usually very fast. Here the limiting process could be either Absorption of CO_2 or the Migration of HCO_3^-. To identify the limiting process, we have compared the rates of CO_2 absorption in the organic solution (i.e., process i) with the rate of CO_2 migration (i.e., process iii). The rates of CO_2 absorption in MAMG process were obtained from previously published data.[1] The data for CO_2 removal rates (or migration rates) are already provided in Figure 6A of the main article. From the figure S3 below, it is observed that the CO_2 absorption rates are much higher than the rates of CO_2 removal from the organic solution. In other words, the rate at which CO_2 migrates in the form of bicarbonate ions remains lower than the CO_2 absorption rate. This indicates that MAMG CO_2 capture process is not mass transfer limited due to CO_2 absorption.

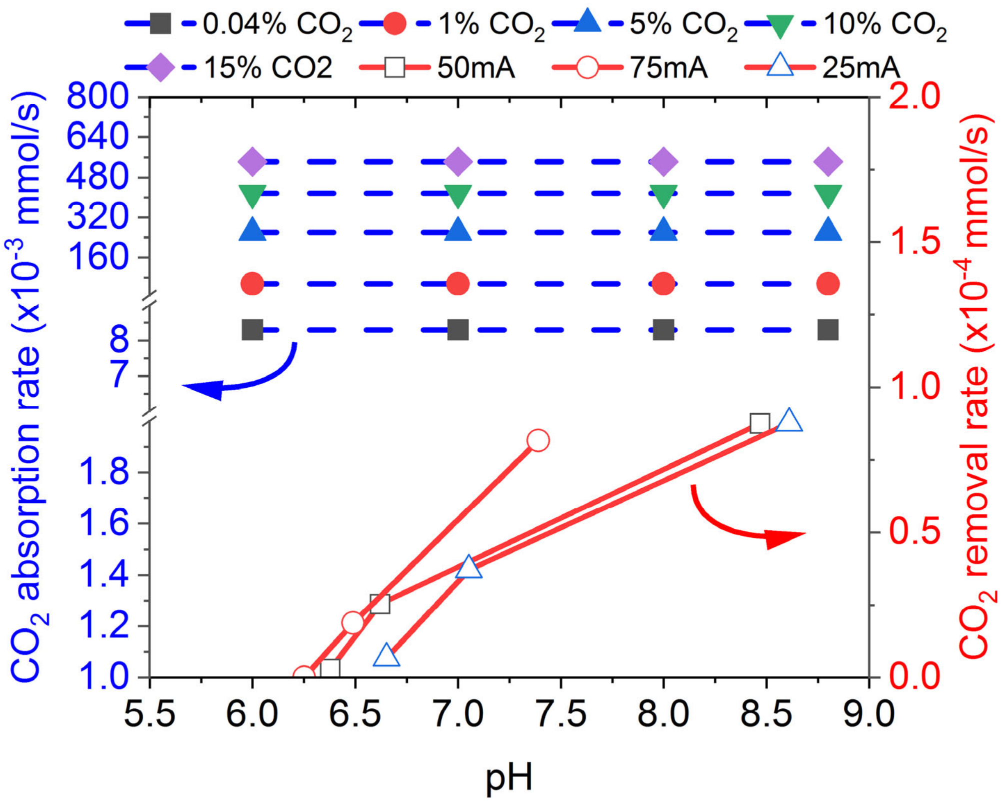

Figure S 3: CO_2 removal rate (defined as the rate of HCO_3^- transfer from organic solution to aqueous solution) of the MAMG process versus pH of the aqueous solution (see the red data lines corresponding to right y-axis). The rates of CO_2 gas absorption in the organic solution for different mole% of CO_2 in N_2 gas (see blue dashed lines corresponding to left y-axis). Since the CO_2 gas absorption rate are at least an order of magnitude higher than the CO_2 removal rates, the MAMG process is not mass transfer limited.

S3. Calculation of dissolved CO_2, gaseous CO_2, and total carbon balance

Dissolved CO_2: MAMG CO_2 capture performance was measured by observing the drop in the pH on the aqueous side due to the migration of HCO_3^- and its conversion to CO_2 and CO_3^{2-}. Using the well-established aqueous equilibrium relationship of these species, the CO_2 concentration was calculated using pH as follows:

The equilibrium constants are obtained from these aqueous reactions:

$$CO_2 + OH^- \leftrightharpoons HCO_3^- \quad (K_{1,aq} = 10^{7.63}\ l/mol)$$
$$CO_2 + H_2O + CO_3^{2-} \leftrightharpoons 2HCO_3^- \quad (K_{2,aq} = 10^{3.88}) \tag{1}$$

Using the above relationship, the HCO_3^- and CO_3^{2-} concentrations can be expressed in terms of CO_2 as:

$$[HCO_3^-] = K_{1,aq} \times [CO_2][OH^-] \tag{2}$$

$$[CO_3^2-] = \frac{[HCO_3^-]^2}{K_{2,aq} \times [CO_2]} = \frac{\left(K_{1,aq} \times [CO_2][OH^-]\right)^2}{K_{2,aq} \times [CO_2]} = K_{1,aq}^2 \times \frac{[CO_2][OH^-]^2}{K_{2,aq}}$$

Imposing electroneutrality on the aqueous side, the total ionic balance can be written as:

$$\Sigma_i z_i C_i = 0 \qquad (3)$$

where z_i is the charge of the ionic species and C_i is the concentration of the species. The electroneutrality equation can be expressed in terms of the ionic species on the aqueous side as:

$$[K^+] + [H^+] - [OH^-] - [Cl^-] - [HCO_3^-] - 2[CO_3^{2-}] = 0$$

$$[K^+] + [H^+] - [OH^-] - [Cl^-] - K_{1,aq} \times [CO_2][OH^-] - 2K_{1,aq}^2 \times \frac{[CO_2][OH^-]^2}{K_{2,aq}} = 0 \qquad (4)$$

The only unknown in eq. (4) is $[CO_2]$ as $[K^+] = 0.775M$ and $[Cl^-] = 0.75\ M$ being the spectator ions that don't participate in the equilibrium reactions, $[H^+] = 10^{-pH}M$, and $[OH^-] = 10^{pH-14}M$.

Gaseous CO_2: The concentration of the gaseous CO_2 was determined by Ar sweeping the headspace of the aqueous reservoir of the MAMG CO_2 capture system into GC. As the aqueous solution reaches saturation pH, the HCO3- migrating from the organic side to the aqueous side can no longer be held as dissolved CO_2 and, therefore, bubbles out as gaseous CO_2. When the primary charge carrier anion in the organic side is HCO3-, the total HCO3- transferred can be given as:

$$[C] = \frac{I_m \times t}{F} \qquad (5)$$

where $[C]$ is the total carbon transferred from the organic side to the aqueous side, $I_m\ (mA)$ is the migration current, t is the duration of the MAMG CO_2 capture experiment, and $F = 96485\ C/mol$ is Faraday's constant. Theoretically, the gaseous CO_2 evolved can be obtained by:

$$\left[CO_{2(g)}\right] = [C] - (\left[CO_{2(aq)}\right] + [HCO_3^-] + [CO_3^{2-}]) \qquad (6)$$

where $[C]$ is obtained from equation (5), $\left[CO_{2(aq)}\right], [HCO_3^-], and\ [CO_3^{2-}]$ are obtained from pH using equation (4). Figure S 4 shows a comparison of the theoretical and the experimental gaseous CO_2 evolved during the MAMG CO_2 capture process. It is clear from this figure that the experimental value follows closely with the theoretical value and thus, accounts for all the carbon migrating from the organic side to the aqueous side. This further supports the assumption that the pH drop in the aqueous solution is only due to the HCO_3^- migrating and getting converted to dissolved CO_2.

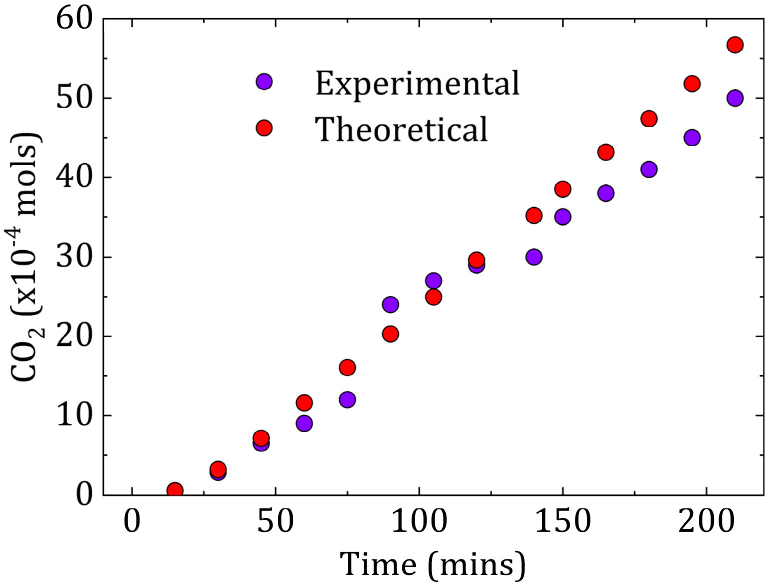

Figure S 4: Comparison of the theoretical gaseous CO_2 released from the MAMG process vs. the experimental CO_2 released monitored through GC.

S4. pH of the electrolyte at various partial pressures of CO_2

The equilibrium pH of the electrolyte depends on the partial pressure of CO_2 by Henry's law. Therefore, the effect of pH on CO2RR experiments was studied by varying the partial pressures of CO_2 for 100 sccm of total gas sparging into the electrolyte solution. The equilibrium concentration of CO2 is related to its partial pressure as:

$$[CO_2] = H \times P_{CO_2} \tag{7}$$

where $H = 33mM/atm$ is the Henry's constant, and P_{CO_2} is the partial pressure of CO_2. The total flow rate of the sparged gas was maintained at 100 sccm, and the fraction of CO_2 was balanced with Ar at different pH. Table S 2 shows how varying the partial pressure of CO_2 affected the pH.

Table S 2: Data showing the flow rate of CO_2 used to maintain constant pH to study CO2RR at different pH.

pH	P_{CO_2}	**CO_2 flow rate (sccm)**	**Ar flow rate (sccm)**
6.2	1	100	0
7.2	0.1	10	90
8.2	0.01	1	99
9.2	0.001	0.1	99.9

S5. Rate of CO_2 addition as a function of pH

While working with a pseudo-integrated process of CO2RR and the controlled addition of CO_2, we identified that sparging pure CO_2 at various flow rates into the electrolyte affects the rate at which the CO_2 is dissolved in the solution. The pH saturation at higher flow rates like 20 sccm is faster compared to slower flow rates like 5 sccm. The rate of CO_2 addition is also dependent on the pH of the electrolyte as it nears saturation. Initially, when the CO_2 concentration is negligible in the electrolyte, the rate of CO_2 addition is constant and is virtually independent of the pH. However, the slope of the rate changes as the saturation pH approaches. This behavior is important to visualize as it indicates the rate at which CO_2 is added to the solution near saturation pH for varying flow rates. Subsequently, this information is also helpful in calculating the net CO_2 removal rate from the pseudo-integrated CO2RR with a controlled CO_2 addition process. Figure S 5 shows this cross-plot visualization between the CO_2 addition rate and pH from the data obtained for pH vs. time and CO_2 addition rate vs. time in the controlled CO_2 addition experiments.

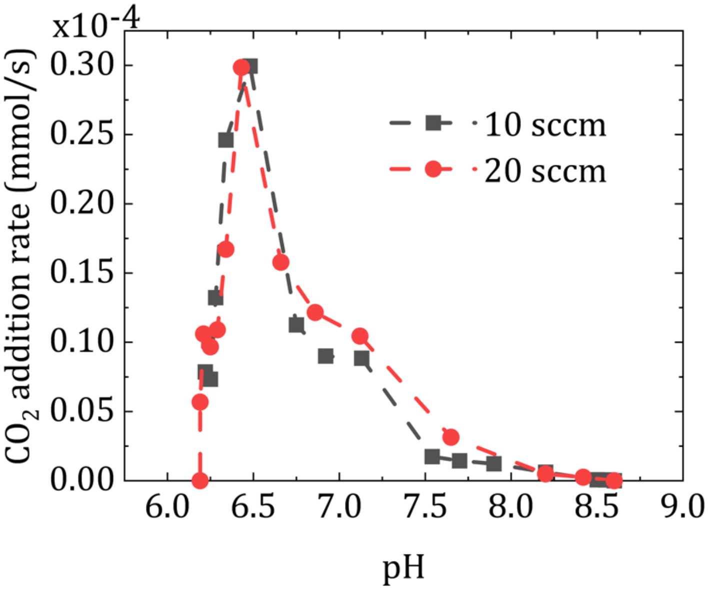

Figure S 5: A cross-plot of the CO_2 addition rate determined in the manuscript vs. pH

S6. Physical map of an integrated system with MAMG CO_2 capture and electrochemical CO2RR

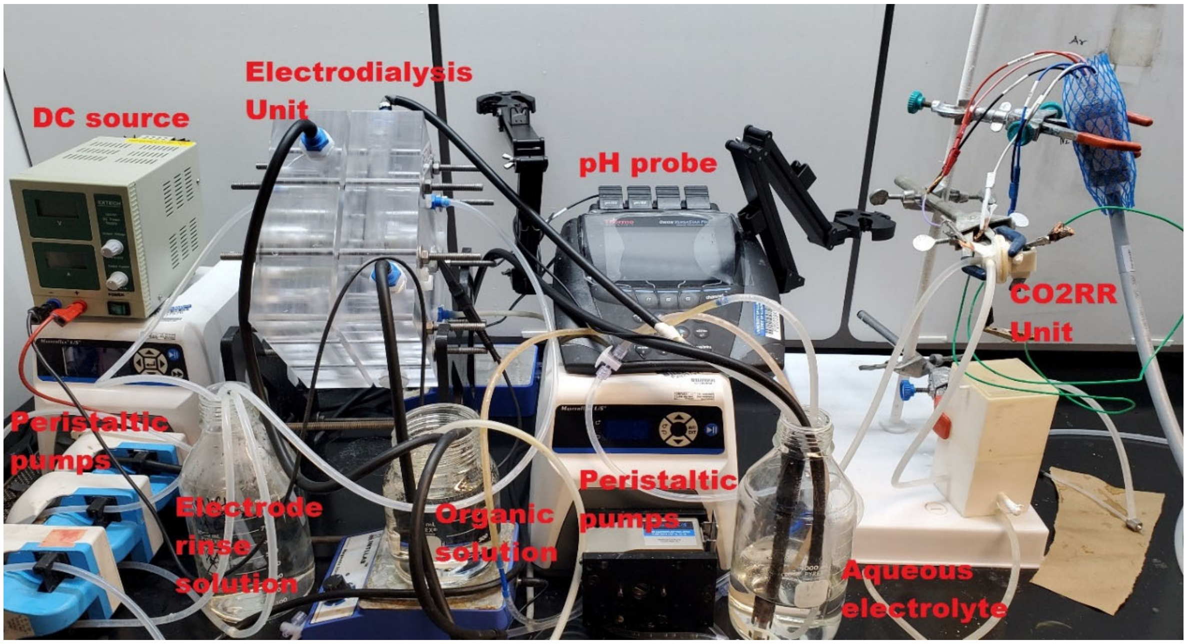

Figure S 6: A physical picture of the integrated system with MAMG CO_2 capture and electrochemical CO2RR

S7. Stability of Large-Scale Integrated Setup with MAMG CO_2 capture and Electrochemical CO2RR

To demonstrate the robustness the integrated setup was run with an Electrodialysis (ED) unit and a CO2RR unit. The ED unit comprised of alternating membranes of Anion exchange membrane and Bipolar membranes. Electrode rinse solution was aqueous 1M KOH solution. A constant migration current (I_m) of 600mA was employed to power the ED unit. Additional details of the working of MAMG CO_2 capture with ED unit can be found in our previous work[1, 2]. The aqueous electrolyte solution comprised of 0.75M KCl and 0.025M $KHCO_3$ pre-equilibrated with CO_2 at a pH of 7.0. Organic side consisted of a KOH saturated solution of ethylene glycol and choline hydroxide acting as the organic CO_2 binding organic liquid (CO2BOL). A simulated flue gas of 10% CO_2 and 90% N_2 was sparged in the CO2BOL reservoir. The CO2RR experiments were conducted in a 3D printed electrochemical cell with a 3D Cu mesh as the cathode and a Nickel foam as anode. A Fumasep FBM-PK membrane in reverse bias mode separated the working and the counter compartment of the electrochemical cell. The anolyte for the CO2RR unit was aqueous 3M KOH solution. A chronopotentiometry experiment for CO2RR was run in an oscillation mode at reduction current density (I_{red}) of 200mA/cm^2 and oxidation current density (I_{oxd})of 2mA/cm^2 with a switching time (t_{switch}) of 2 seconds. Additional details about the oscillation experiments can be found in our previous work [3] Product gases were collected in a gas bag (30 min at 25 sccm) using Ar as the carrier gas and resultant products were quantified using a gas chromatograph (GC, SRI8610C).

References

1. A. Prajapati, R. Sartape, T. Rojas, N. K. Dandu, P. Dhakal, A. S. Thorat, J. Xie, I. Bessa, M. T. Galante and M. H. Andrade, *Energy & Environmental Science*, 2022, **15**, 680-692.
2. R. Sartape, A. Prajapati, N. C. Kani, T. Rojas, N. K. Dandu, P. Dhakal, A. S. Thorat, J. Xie, I. Bessa and M. T. Galante, *Energy & Environmental Science*, 2022, **15**, 3994-3996.
3. A. Prajapati, N. C. Kani, J. A. Gauthier, R. Sartape, J. Xie, I. Bessa, M. T. Galante, S. L. Leung, M. H. Andrade and R. T. Somich, *Cell Reports Physical Science*, 2022, **3**, 101053.